NASA/TM-20220001809

An Investigation Into Some Important Aspects of Droplet Breakup/Vaporization Behavior Caused by a Gas Flow (Both Nonreacting and Detonative Combustion) in a Shock Tube

M.S. Raju
HX5, LLC, Brook Park, Ohio

Kenji Miki
Glenn Research Center, Cleveland, Ohio

April 2022

NASA STI Program . . . in Profile

Since its founding, NASA has been dedicated to the advancement of aeronautics and space science. The NASA Scientific and Technical Information (STI) Program plays a key part in helping NASA maintain this important role.

The NASA STI Program operates under the auspices of the Agency Chief Information Officer. It collects, organizes, provides for archiving, and disseminates NASA's STI. The NASA STI Program provides access to the NASA Technical Report Server—Registered (NTRS Reg) and NASA Technical Report Server—Public (NTRS) thus providing one of the largest collections of aeronautical and space science STI in the world. Results are published in both non-NASA channels and by NASA in the NASA STI Report Series, which includes the following report types:

- TECHNICAL PUBLICATION. Reports of completed research or a major significant phase of research that present the results of NASA programs and include extensive data or theoretical analysis. Includes compilations of significant scientific and technical data and information deemed to be of continuing reference value. NASA counter-part of peer-reviewed formal professional papers, but has less stringent limitations on manuscript length and extent of graphic presentations.

- TECHNICAL MEMORANDUM. Scientific and technical findings that are preliminary or of specialized interest, e.g., "quick-release" reports, working papers, and bibliographies that contain minimal annotation. Does not contain extensive analysis.

- CONTRACTOR REPORT. Scientific and technical findings by NASA-sponsored contractors and grantees.

- CONFERENCE PUBLICATION. Collected papers from scientific and technical conferences, symposia, seminars, or other meetings sponsored or co-sponsored by NASA.

- SPECIAL PUBLICATION. Scientific, technical, or historical information from NASA programs, projects, and missions, often concerned with subjects having substantial public interest.

- TECHNICAL TRANSLATION. English-language translations of foreign scientific and technical material pertinent to NASA's mission.

For more information about the NASA STI program, see the following:

- Access the NASA STI program home page at http://www.sti.nasa.gov

- E-mail your question to help@sti.nasa.gov

- Fax your question to the NASA STI Information Desk at 757-864-6500

- Telephone the NASA STI Information Desk at 757-864-9658

- Write to:
  NASA STI Program
  Mail Stop 148
  NASA Langley Research Center
  Hampton, VA 23681-2199

NASA/TM-20220001809

An Investigation Into Some Important Aspects of Droplet Breakup/Vaporization Behavior Caused by a Gas Flow (Both Nonreacting and Detonative Combustion) in a Shock Tube

M.S. Raju
HX5, LLC, Brook Park, Ohio

Kenji Miki
Glenn Research Center, Cleveland, Ohio

National Aeronautics and
Space Administration

Glenn Research Center
Cleveland, Ohio 44135

April 2022

Acknowledgments

This work was supported by NASA's Transformational Tools and Technologies project. M.S. Raju would like to extend his sincere thanks to Dr. Jeff Moder for his continued support and Drs. D. Perkins and S. Youngster for providing valuable insights during this investigation.

This work was sponsored by the
Transformative Aeronautics Concepts Program.

Level of Review: This material has been technically reviewed by technical management.

This report is available in electronic form at http://www.sti.nasa.gov/ and http://ntrs.nasa.gov/

An Investigation Into Some Important Aspects of Droplet Breakup/Vaporization Behavior Caused by a Gas Flow (Both Nonreacting and Detonative Combustion) in a Shock Tube

M.S. Raju
HX5, LLC
Brook Park, Ohio 44142

Kenji Miki
National Aeronautics and Space Administration
Glenn Research Center
Cleveland, Ohio 44135

ABSTRACT

As a part of the rotating detonation engine (RDE) technology enablement project at NASA Glenn Research Center (GRC), an effort was undertaken to extend our current computational capabilities of OpenNCC in some important ways with the implementation of a modeling approach to account for the droplet breakup caused by a shock-induced gas motion, & a vaporization model valid over a wide range of pressure conditions encountered in multiphase detonation.

With the modified code, a study was undertaken to investigate the individual droplet behavior followed by the passage of a shock front. The study is carried out by tracking a sparse group of droplets to gain some understanding of shock induced droplet behavior under various shock strengths & fuel injector conditions. The study also looks into the effect of randomization involved in determining the droplet breakup outcomes. Over a wide range of sub-critical conditions examined, larger droplets are observed to undergo significant changes in droplet behavior following their breakup. However, smaller droplets (10 μm or less) remain unaffected by any shock induced breakup.

In a follow-on work, we investigated the impact of shock and droplet interaction in a detonation study involving both gaseous as well as gas/liquid (droplet clouds) fuel/air stoichiometric mixtures in a simple 3D shock-tube configuration. The droplet clouds are made up of different initial droplet sizes of either 6, 10, or 30 μm. We also investigated the individual droplet behavior followed by the passage of a detonation front. The results represent conditions that lead to both overdriven and C-J (Chapman-Jouguet) detonations. Under both test conditions, most of the droplet vaporization is completed within a short distance (duration) behind the detonation front & well within the region of complete combustion observed in a corresponding equivalent gas-phase fuel/air mixture. The impact of the shock-induced droplet breakup is found to be significant in the calculations involving the 30-μm droplets. Subsequent to the breakup, the drop sizes vary from 1 to 10 μm. Another factor that contributed to the observed rapid vaporization is the result of vaporization taking place under supercritical conditions. The overall detonation properties of various droplet clouds (made up of different initial sizes) are similar to those observed in a corresponding gaseous fuel/air mixture. In the calculation involving a gaseous fuel, the calculated C-J detonation velocity is 1822 m/s involving Jet-A/air and $\phi = 1$. In the overdriven detonation, it is 2044 m/s. In the calculations involving droplet clouds, the corresponding detonation velocities are lower. The impact of increased droplet size is primarily seen in a higher reduction in the detonation velocity.

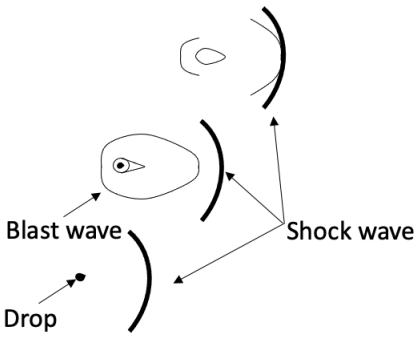

Fig. 1 Schematic of the interaction between blast waves generated from a droplet and the shock front [1].

1. INTRODUCTION

In gaseous detonations, the energy release is continuous after an induction time [1]. In multiphase detonation, it takes place in a discrete manner at the site of droplets [2]. The local explosions originating from droplets set off blast waves [1-2]. The main front is reinforced with the additional energy release as these waves catch up with the main front [1-2]. A schematic of Dabora's interpretation of the interaction between blast waves generated from a droplet and the shock front are shown in Fig. 1 [1]. However, the shock waves moving in opposite direction reduces some of the total energy available to support the detonation front. This could explain the reduced velocity deficit observed in spray detonation [3]. The location of the local explosions behind the shock front seemed to vary depending on droplet sizes with smaller droplets causing explosions closer to the front and vice versa [3]. The experiments also seemed to indicate the developmental time required for spray detonation to reach a steady state decreases with smaller droplet sizes [2]. More importantly, the detonation wave propagates slower than the equivalent gas-phase C-J velocity and the observed velocity deficit being a function of droplet size with higher drop sizes producing a larger deficit [3].

The physics associated with both the location and origin of local explosions is more complicated. Because of the steep rise in velocity and other thermodynamic properties followed by the passage of a leading shock front, the droplet is subjected to a strong deformation due to the formation of a bow shock at the front. Several other shocks are also formed in its wake region as observed in the experiments of [4]. More importantly, the actual location of explosions was observed to occur in the unreacted wake of a lead droplet somewhere in the mid-region of the wake formed with other interacting downstream droplets. It is where after the built-up of a sufficient reacting fuel/air mixture, an explosive event sets off strong shock waves whose initial structure is spherical [4].

Numerous experimental studies were undertaken to gain some understanding of ignition/detonation properties of various hydrocarbon-air mixtures [5-8]. The impact of both evaporating droplets & solid particles on ensuing shock structure was reported in several numerical investigations [3, 9-11]. They are undertaken mostly to gain some understanding of shock/detonation properties in a droplet/particle cloud [12-15]. Recently, Hayashi et al. [16] presented a numerical study of JP-10/air detonation involving a RDE application.

In the present paper, we attempt to provide some understanding into the individual droplet behavior followed by the passage of a shock front, and the impact of shock induced droplet breakup in a multiphase detonation. Based on several studies undertaken within the context of individual droplet behavior, the impact of shock induced aerodynamic shattering and breakup of liquid drops was well investigated [17-19]. However, its importance and understanding is not well documented in the reported CFD calculations relevant to PDE (Pulse Detonation Engine)/RDE applications. First, we are going to describe the details of modeling approach that we employed. The details of our current spray modeling is well documented in LSPRAY-V [20]. In this paper, we describe mainly the modifications we implemented to account for the shock-induced droplet breakup & vaporization valid over a wide range of likely conditions encountered in PDE/RDE applications.

2. DETAILS OF OUR MODELING APPROACH FOR DROPLET SHATTERING AND BREAKUP CAUSED BY A SHOCK INDUCED GAS FLOW

In an effort to extend our current computational ability, we decided to implement a modeling approach based on the shock-induced droplet breakup criteria developed by Borisov et al. [3]. It helps us determine various droplet breakup outcomes based on the instabilities widely identified by parachute-type or chaotic breakup, droplet stripping, & explosive breakup depending on a criteria established by a set of Reynolds and Weber numbers in a given flow regime. More importantly, it provides the characteristic times associated with different kinds of droplet

breakup. In our current implementation, the actual outcomes after the breakup are determined by the existing RT (Rayleigh-Taylor) and ETAB (Enhanced Taylor Analogy Breakup) secondary droplet breakup models as described in LSPRAY-V [20].

Based on an analysis of extensive experimental data, Borisov et al. [3] identified the following set of unique droplet breakup regimes:

$$\textbf{(I)} \ \begin{cases} 4 \leq We \leq 20, \\ 0.1 \leq WeRe^{-0.5} \leq 0.3; \end{cases} \quad (1)$$

$$\textbf{(II)} \ \begin{cases} 10 \leq We \leq 10^4, \\ 0.5 \leq WeRe^{-0.5} \leq 10; \end{cases} \quad (2)$$

$$\textbf{(III)} \ \begin{cases} 10^3 \leq We \leq 10^5, \\ 10 \leq WeRe^{-0.5} \leq 10^2; \end{cases} \quad (3)$$

where the Weber number, We, characterizes the impact of aerodynamic forces on droplet deformation and the criterion, $WeRe^{-0.5}$, describes the conditions necessary for breakup associated with the removal of liquid from the surface layer. This classification is established based not only on the physical pattern of droplet breakup but also on an analysis of the spectrum of the new droplets being formed. In Regime I, the secondary droplets have dimensions closer in magnitude to the size of the original droplets. It leads to the formation of droplets into two or more parts based on the parachute type and chaotic breakup. In Regime II, the surface layer is torn off in the form of droplet stripping. It leads to the formation of a parent droplet closer in dimension to the original droplet along with a significant fraction of very fine droplets. In Regime III, it leads to the explosive breakup of the droplets which leads to the formation of significantly smaller droplets.

Based on Borisov et al. [3], the characteristic time intervals associated with various regimes are determined. They are required to determine the possibility of realizing one or the other type of breakup. For the case of sudden loading by aerodynamic forces, e.g., behind a shock wave, the time for droplet deformation to the critical stage (i.e., the stage at which its perforation by instability waves commences) associated with the bag (also referred to as parachute-type or chaotic) breakup mode, t_{bag}, is given by

$$t_{bag} \ = \ du^{-1}(\frac{\rho_l}{\rho_g})^{0.5} \quad (4)$$

The characteristic boundary-layer establishment time associated with the boundary layer stripping (BLS) breakup mode is given by

$$t_{BLS} \ = \ 0.36du^{-1}(\frac{\rho_l}{\rho_g})^{0.5} \ = 0.36t_{bag} \quad (5)$$

The characteristic time for increase in perturbation amplitude on the liquid surface due to Rayleigh-Lamb-Taylor instability (RLT) is same as t_{bag} & the corresponding droplet destruction time to explosive decay is given by

$$t_{RLT} \ = \ 10 \, t_{bag} \, We^{-0.25} \quad (6)$$

Finally, there is another important time scale associated with characteristic droplet acceleration time (DAT) as given by

$$t_{DAT} \ = \ \frac{4\rho_l d}{3c_x\rho_g u} \ = \ 4(\frac{\rho_l}{\rho_g})^{0.5}\frac{t_{bag}}{3c_x} \quad (7)$$

c_x has a value of 1.0 to 2.0. At atmospheric pressure ($\rho_l\rho_g^{-1} >> 1$), the droplet acceleration time is much greater than droplet breakup. However, at higher pressures it becomes comparable to the time scales associated with deformation.

It is important to note that the characteristic time intervals represent the minimum time period needed for any breakup outcome to be realized after which the actual droplet-breakup outcome is determined by the corresponding regime as identified by We and $WeRe^{-0.5}$ in Eqs. 1-3. However, it should be noted that the actual droplet breakup becomes a possibility only if the rate-controlling time event is less than t_{DAT}.

After a significant droplet breakup event, individual drop vaporization is likely to take place mostly in a shock-free environment. It is because the resulting child (smaller) droplets tend to accelerate much faster. In a multi-phase detonation regime of our interest, the characteristic times associated with droplet breakup represent only a small fraction of the overall droplet vaporization time. Therefore, the individual droplet behavior based on our current modeling approach employed in [20] is likely to provide a reasonable representation.

The actual outcomes following a droplet breakup are determined by making use of the ETAB model [21-22] for the regimes identified by I & II, and the RT model [23] for Regime III. More details on the ETAB & RT secondary droplet breakup models can be found in LSPRAY-V [20]. In summary, the framework that we employed makes use of the existing secondary droplet breakup models in LSPRAY-V

[20] based on the droplet-breakup time criteria identified by [3].

3. IMPLEMENTATION OF A VAPORIZATION MODEL VALID OVER A WIDE RANGE OF PRESSURE CONDITIONS ENCOUNTERED IN MULTI-PHASE DETONATION

In a shock tube configuration, some vaporization takes place under normal pressure conditions. But the pressures behind a shock or detonation front tend to be much higher & may even exceed supercritical pressure. It can lead to significant changes in droplet behavior. For example, higher boiling temperature resulting from the pressure gain can lead to a significant increase in the droplet heating period.

LSPRAY-V has separate vaporization models valid over a wide range of different conditions (normal, superheat & supercritical). For a PDE simulation, we need a capability to switch between normal and supercritical conditions. The coding needed for this requirement was completed. To be consistent with the supercritical vaporization model, a simple infinity conductivity model is invoked in calculating the internal droplet liquid temperature [20].

To make use of the supercritical vaporization model, a table needs to be created to determine the liquid-phase interface conditions for a given specified pressure. In a shock/detonation-tube configuration, the droplets are likely to interact with multiple shocks (incident & reflected). In our current implementation, a single table is generated based on the conditions anticipated behind a detonation front. Further refinement of vaporization models is not anticipated since vaporization becomes very rapid at supercritical pressures.

4. NUMERICAL APPROACH

In an effort to guide in the design and testing of advanced gas-turbine combustors, NASA Glenn research center (GRC) has undertaken the development of OpenNCC. It is mainly developed with the aim of advancing the current multi-dimensional computational tools used in the design of aircraft combustors. Since its inception about more than 20 years ago, the code has gone considerable evolution to accommodate the changing needs of various ongoing projects associated with next-generation combustor technology development. More on the current status of OpenNCC can be found in Refs. [24-26]. It can be used in a numerical investigation of both steady/unsteady, reacting/non-reacting, & gaseous/spray calculations by employing a wide range of relevant numerical schemes & turbulence/chemical-kinetic/spray models.

Fig. 2 Shock tube configuation.

Our present gas-phase computations are based on an unsteady Euler solution with explicit, four-stage Runge-Kutta scheme based on a second-order accurate ausm+-up (MUSCL-tpye, limiter) discretization for inviscid fluxes. More on the spray modeling approach can be found in the LSPRAY-V manual [20].

5. RESULTS & DISCUSSION

5.1 Individual Droplet Behavior Followed by the Passage of a Shock Front Under Non-Reacting Conditions

In this section, we are going to present some results from a study undertaken to gain some understanding of the shock induced droplet behavior. It is carried out by tracking a sparse group of droplets (five to ten) by initially placing them away from the diaphragm in the low-pressure section of a shock tube. Several 3D calculations were performed based on a simple rectangular (0.01m wide and 0.45m long) shock-tube configuration shown in Fig. 2. The driver section is placed in the axial region between 0 to 0.222 m. First we are going to show some results where the high-pressure region is filled with air at 20 atm & 600 K & the low-pressure region with air at 1 atm & 300 K. This test condition leads to the following conditions behind the shock: P_g = 491658 Pa, T_g = 520 K & ρ_g = 3.3 kg/m^3. A specified number of droplet parcels are initially introduced in a random manner from a narrow slit located at an axial location of 0.25 m. The corresponding particle number density

is kept to a very minimum in order to limit any modifications arising from the liquid-phase source-term contribution to the gas-phase to be negligible. Such an arrangement is chosen to ensure vaporization to occur under nearly identical gas-phase conditions. In this section, our attention is focussed mainly on the following aspects of shock induced droplet behavior:

- Introduce a group of droplets based on some widely-used droplet-size distributions to gain some understanding under different injector conditions.
- Introduce a group of the same droplet sizes to gain some understanding of randomization involved in determining the droplet breakup outcomes.
- Examine droplet behavior at different shock strengths.

The time variation of droplet size, axial velocity, temperature, & axial location are shown in Fig. 3. The results are based on a group of five droplets chosen to represent an injector condition based on the droplet-size distribution (DSD) of Banhawy et al. [20] with a Sauter mean diameter (SMD) of 12 μm. The resulting initial droplet sizes are comprised of 5, 10.5, 17.4, 24.5, & 31.7 μm, & the percentage of liquid mass contained within each group is given by 13.2, 38.5, 27.2, 14.4, & 6.6, respectively. It is obvious from the time variation of droplet size, only 4 out of 5 larger droplets experience breakup and the breakup happens only once subsequent to the passage of an incident shock. Subsequent to the breakup, the droplet sizes vary from 1 to 10 μm. At the time of one such a typical droplet breakup event, the calculated breakup times associated with various breakup modes (as identified by Eqs. 4-6) are t_{bag} = 6.24e-7, t_{BLS}, = 2.24e-7, & t_{RT} = 2.54e-6. It is important to note that the droplet acceleration time (t_{DAT} = 1.42e-5 s) exceeds all other breakup times and thereby ensuring an inevitable breakup outcome. Also, as expected the rate controlling mode for this eventual breakup event is BLS.

Subsequent to the passage of the incident shock, the time variation of droplet axial velocity shows the expected particle behavior with the smaller particles accelerating faster. While the smallest droplets (1μm fragments formed after the breakup) accelerate much faster, the larger ones lag progressively behind. Near their end of complete vaporization, the droplet velocities approach closer to the calculated gas velocity of about 480 m/s. Also as expected, the droplet surface temperature variation shows the smaller droplets heat up much faster. The surface temperature of the 1-μm droplet raises much faster and reaches close to the boiling temperature of 430^o K. The time that it takes for it to reach near boiling temperature is about 0.002 ms, and it is 0.004 ms for complete vaporization. However, it is important to note that all of the droplet vaporization takes place in a very low surrounding gas temperature. It is because the gas temperatures before and after the passage of the shock front are 300 and 520 K, respectively. Meanwhile within the calculation time period of 0.006 ms, the droplet surface temperatures of the remaining 3, 5, & 10 μm droplets reach about 400, 365, & 333 K, respectively. For comparison purposes in a typical sub-critical flame (gas-turbine) environment, it takes about 0.1 ms for a 10-μm droplet to vaporize completely. Also, the time variation of axial droplet location exhibits a familiar pattern with smaller particles staying closer to the shock front as they accelerate faster. The larger ones lag progressively behind with increased droplet size.

Shown in Fig. 4 is the time variation of droplet size, axial velocity, temperature, & axial location for an injector condition based on the same DSD of Banhawy et al. [20] but with a smaller SMD of 8.8 μm. This fuel injector condition was used in one of our prior calculations involving soot emissions generated by a partially-fueled gas-turbine engine combustor [26]. The resulting initial droplet sizes comprised of 3.64, 7.64, 12.75, 18.06, & 23.27 μm and the percentage of liquid mass contained within each group is given by 12.8, 38.0, 28.6, 14.0, & 6.5, respectively. Again as in the previous calculation, only those droplets larger than 10 μm undergo significant breakup (but only once) subsequent to the passage of an incident shock. Subsequent to the breakup, the droplet sizes vary from 1 to 8 μm. The time variation of corresponding droplet axial velocity, temperature, & axial location shows a familiar behavior with smaller particles showing greater acceleration before approaching the surrounding gas velocity, and they also heat up much faster before approaching the liquid boiling temperature. Next shown in Fig. 5 is the droplet behavior for an injector condition based on the DSD of a clipped PDF [20] with a SMD of 12 μm. The resulting initial droplet sizes comprised of 13.44, 17.28, 16.88, 15.36, & 13.44 μm, and the percentage of liquid mass contained within each group is the same (20%). In this calculation, all the droplets

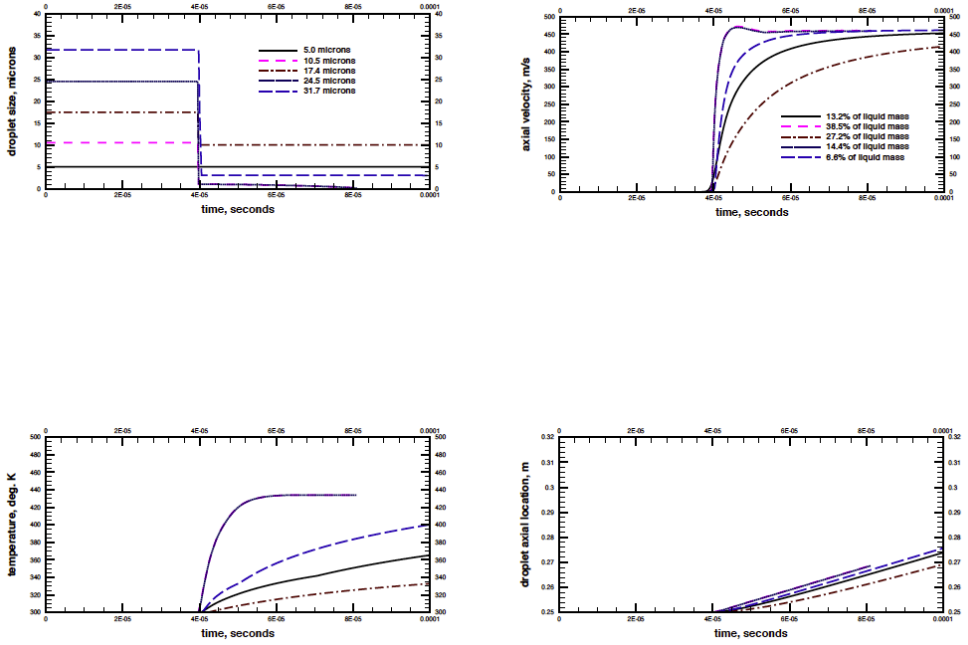

Fig. 3 Shock induced droplet behavior for an injector condition based on DSD of Banhawy et al. [20] with SMD = 15 microns.

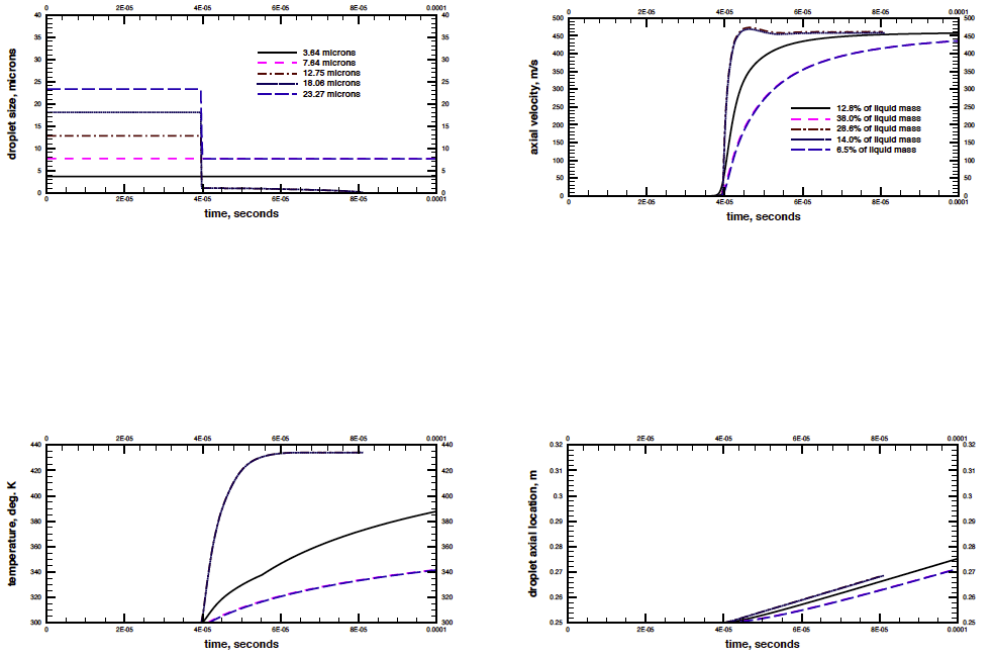

Fig. 4 Shock induced droplet behavior for an injector condition based on DSD of Banhawy et al. [20] with SMD = 8.8 microns.

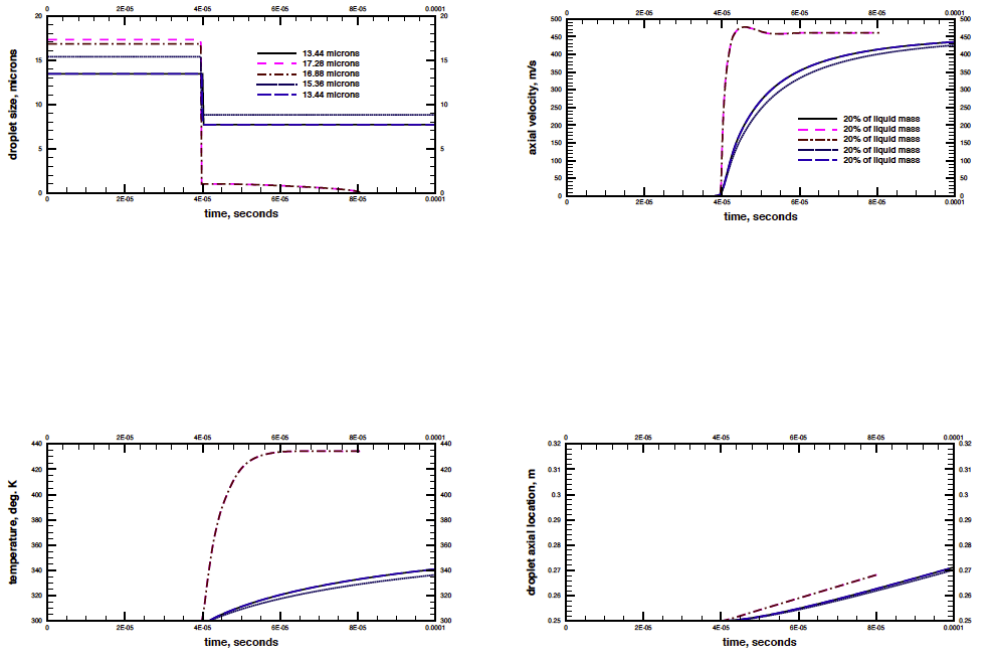

Fig. 5 Shock induced droplet behavior for an injector condition based on DSD of a clipped PDF [20] with SMD = 15 microns.

are seen to undergo breakup. After the breakup, the resulting droplet sizes range between 1 to 9 μm. Once again, the time variation of the corresponding droplet axial velocity, temperature, & axial location exhibits a similar behavior observed in the prior calculations.

In order to gain some understanding of randomization involved in determining the droplet breakup outcomes, we present the results from two calculations obtained by introducing a group of ten droplets of same (equal) size. The results from the 30 & 12 μm droplets are shown in Figs. 6 & 7, respectively. In both calculations, all the droplets are seen to undergo breakup. In the 30-μm calculation after breakup, the resulting droplet sizes range between 5 to 10 μm with few droplets undergoing shattering as indicated by the formation of 1-μm fragments. In the 12-μm calculation, they range between 3 to 7 μm along with few shattered droplets. Again in both calculations, the time variation of corresponding droplet axial velocity, temperature, & axial location show a similar behavior.

In order to gain some understanding of droplet behavior at different shock strengths, we examined droplet behavior by increasing the specified initial pressure in the driver section (of the shock tube shown in Fig. 2) from 20 to 40 atm in one calculation and 100 atm in the second calculation while keeping all other variables the same. The centerline shock profile from the 40-atm calculation is shown in Fig. 8. It shows the axial variation of the gauge pressure, T_g, & Mach number. This test condition leads to the following conditions behind the shock: P_g = 666454 Pa, T_g = 606 K & ρ_g = 3.84 kg/m^3. The time variation of droplet size, axial velocity, temperature, & axial location are shown in Fig. 9. It is based on an injector condition defined by the DSD of Banhawy et al. [20] with a SMD of 12 μm. The resulting droplet-breakup outcomes are similar to those observed earlier with the same injector condition at 20 atm. However, the droplet velocity reaches as high as 600 m/s as a result of higher gas velocity resulting from the increased shock strength. Also, the droplet temperature reaches as high as 470 K. It is because of the increased boiling temperature resulting from higher pressure. All other aspects of droplet behavior is similar to those observed at lower pressure. The centerline shock profile from the 100-atm calculation is shown in Fig. 10. It is also based on the same injector condition. This test condition leads to the following conditions behind the shock: P_g = 972607 Pa,

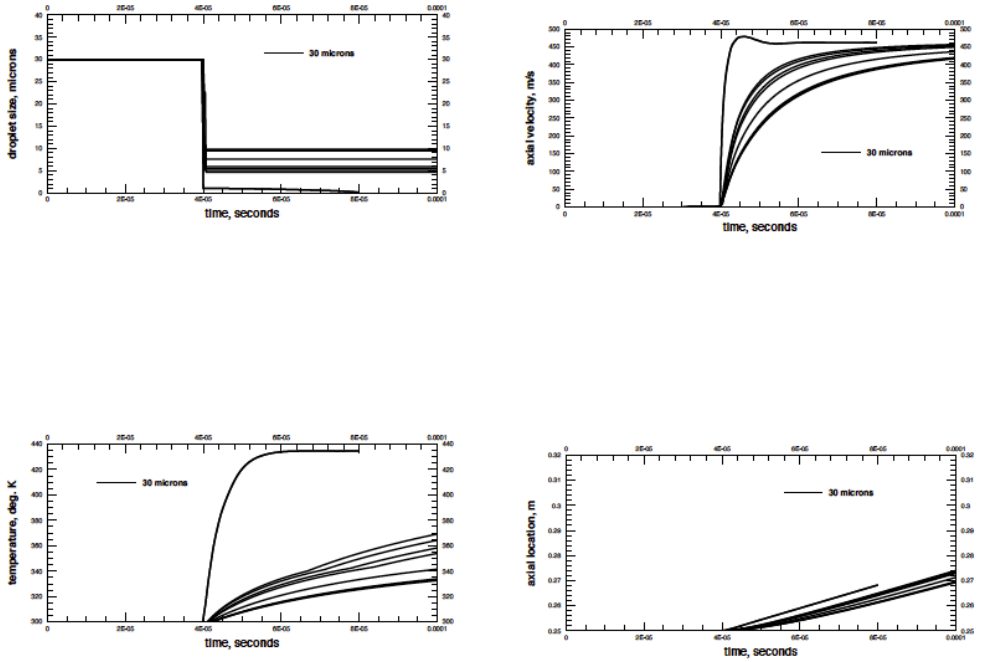

Fig. 6 Impact of randomization on the resulting shock induced droplet breakup outcomes for a group of same initial-size (30 microns) droplets.

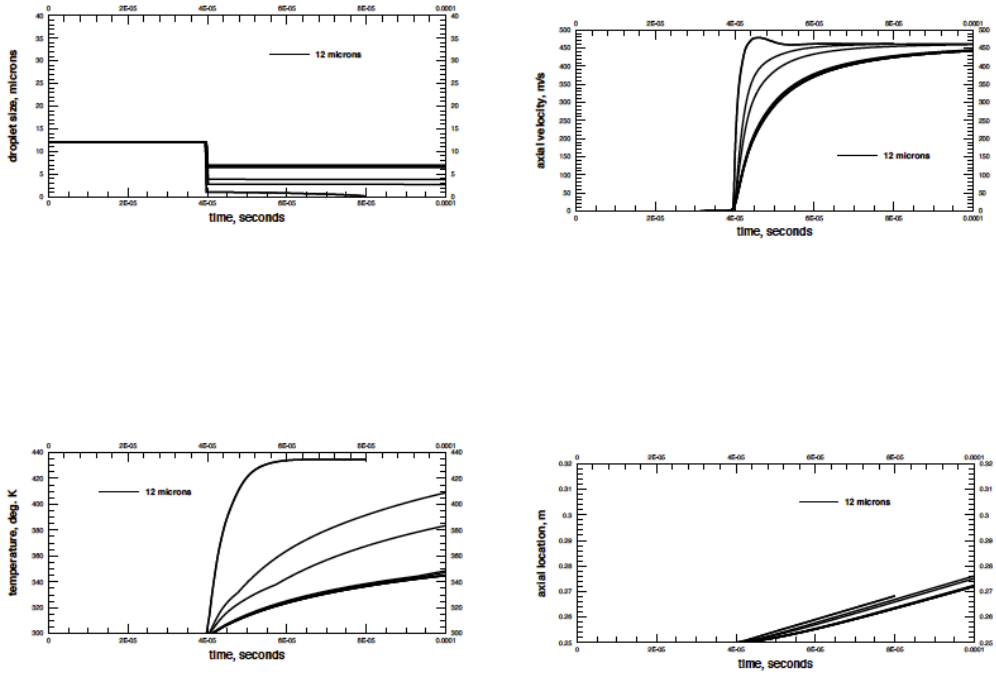

Fig. 7 Impact of randomization on the resulting shock induced droplet breakup outcomes for a group of same initial-size (12 microns) droplets.

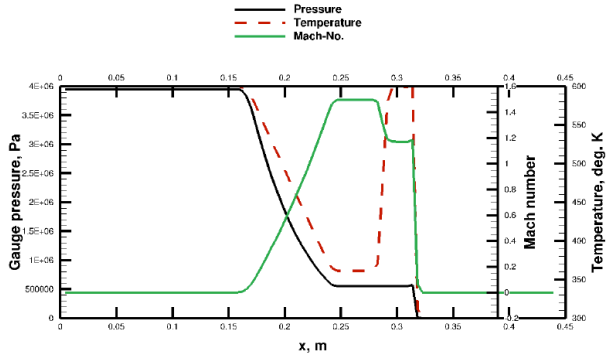

Fig. 8 Centerline shock profile showing variation of P_{gauge}, T_{gas}, & Mach number.

T_g = 747 K & ρ_g = 4.53 kg/m^3. The time variation of corresponding droplet size, axial velocity, temperature, & axial location are shown in Fig. 11. This calculation also shows similar droplet breakup outcomes with two notable exceptions: the drop velocity reaches as high as 770 m/s and the liquid temperature close to 510 K. Again, those differences are a result of further increase in shock strength. Also in both calculations, it is noteworthy that the calculated gas pressures behind the shock are far lower than the critical pressure (about 18.2 atm) of jet-a ($C_{11}H_{21}$) fuel. All the results we presented in this section are based on evaporation taking place in a sub-critical environment.

5.2 Impact of Shock and Droplet Interaction in a Detonation Study involving Droplet Clouds & Individual Droplet Behavior Followed by the Passage of a Detonation Front

In this section, we present the results from a study undertaken to investigate the shock interaction with droplets under reacting conditions. The reacting calculations are based on the reduced chemistry model of Ajmani et al. [27] for Jet-A fuel/air oxidation. However, in our present calculations we removed the NOx related kinetic steps from [27]. The calculations are based on a simulation geometry shown in Fig. 12. Our shock-tube configuration has three distinct axial regions similar to those used by Sommerfeld [28] in his experimental investigation: (1) In order to initiate detonation, the driver section (x = 0 to 0.133 m) is filled with a high energy gas. In the present calculations we present the results from two sets of calculations, one with 200 atm & 2500 K that resulted in overdriven detonation, and the other with 50 atm & 2500 K. that resulted in the C-J detonation velocity; (2) The mid-section (x = 0.133 to 0.5 m) is filled with a gaseous stoichiometric fuel/air mixture at 1 atm & 450 K. The addition of this region is intended to promote the onset of detonation; & (3) The last section (x = 0.5 to 1.5 m) is filled with either a gaseous or mixed-phase medium at 1 atm & 300 K. It is the medium that we are interested in to investigate the shock behavior. As a part of this study we performed several calculations involving a stoichiometric fuel/air mixture. Some are based on a purely gaseous fuel and others are based on a multi-phase (30% gas & 70% liquid) fuel. The multi-phase calculations are based on a droplet cloud made up of different initial droplet sizes (either 6, 10, or 30 microns). Also, in order to gain some understanding of individual droplet behavior, the calculation involving the gaseous fuel continued further after a stable detonation condition was established. In this calculation, the behavior & movement of a sparse group of droplets with initial sizes of 6, 10, & 30 microns is examined followed by after their introduction once before an incoming detonation front.

All the calculations were run until a stable detonation velocity was achieved. Most of the results presented in this section are based on the prevailing flow properties near the end of a calculation.

Overdriven Detonation

In this section, we present the results obtained based on a higher pressure test condition of 200 atm in the driver section of the shock tube.

Results Involving a Gaseous Fuel/Air Mixture

The contour plots of plots of gauge pressure, axial velocity, & temperature, & OH from the calculation involving a gaseous stoichiometric fuel/air mixture are shown in Fig. 13. As expected, both the velocity and pressure remain fairly uniform in the region between the detonation front and the contact surface. A slight step increase in temperature observed towards the tail end of this region (downstream of the contact surface) could be attributed to

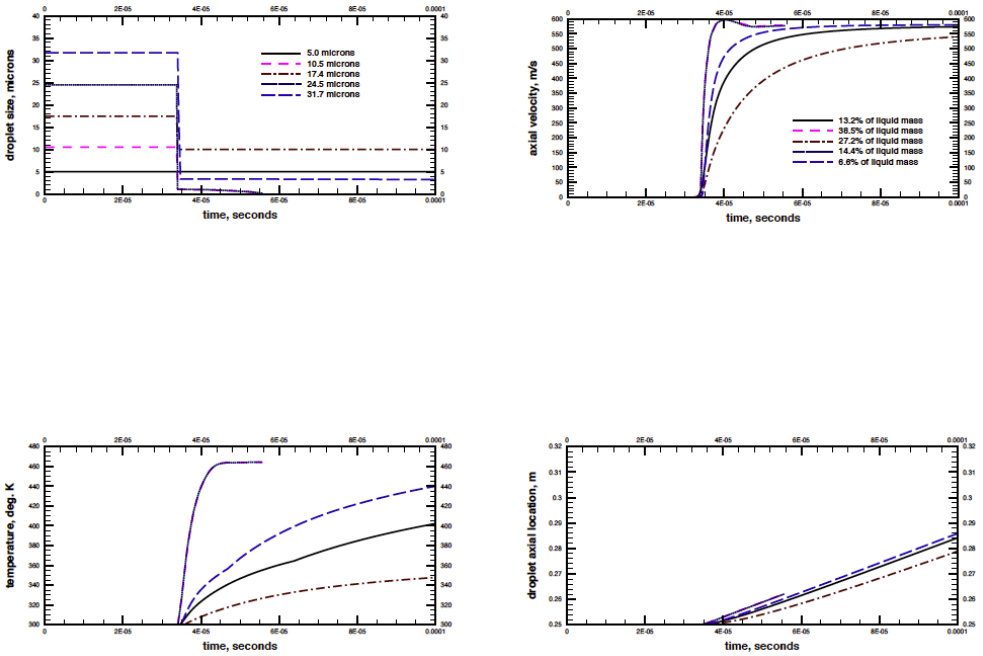

Fig. 9 Shock induced droplet behavior for an injector condition based on DSD of Banhawy et al. [20] with SMD = 15 microns.

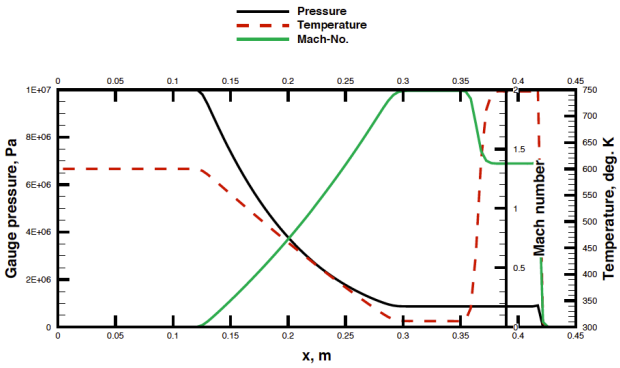

Fig. 10 Centerline shock profile showing variation of P_{gauge}, T_{gas}, & Mach number.

differences in the specified initial temperature in different sections of the low pressure region. Behind the shock front, a a thin region of high reaction activity is formed as noticed in the OH contour plot. The preheat zone thickness appears to be slightly less than 2 mm. There is some evidence of further combustion taking place upstream before it reaches equilibrium flame temperature. It takes about 4 cm for the gas to reach its equilibrium flame temperature behind the shock front. The corresponding centerline shock profile of gas-phase gauge pressure, temperature, Mach number, axial velocity, density and C_p are shown in Figs. 14 & 15. It is noteworthy that at other axial locations not shown here, the results for P_g, T_g, & ρ_g are mostly identical but show some minor differences in the flame region. However, behind the detonation front in the flame region, the calculated axial velocity fluctuations are as large as 15%. But they quickly dampen out further upstream of the flame region. Behind the flame region, the calculated values for P_g, T_g, Mach number & axial velocity are about 33 atm, 3400 K, 1, & 1230 m/s, respectively. The calculated detonation velocity is 2040 m/s which is well above the C-J detonation velocity of about 1800 m/s reported by [29] for Jet-A/air at $\phi = 1$.

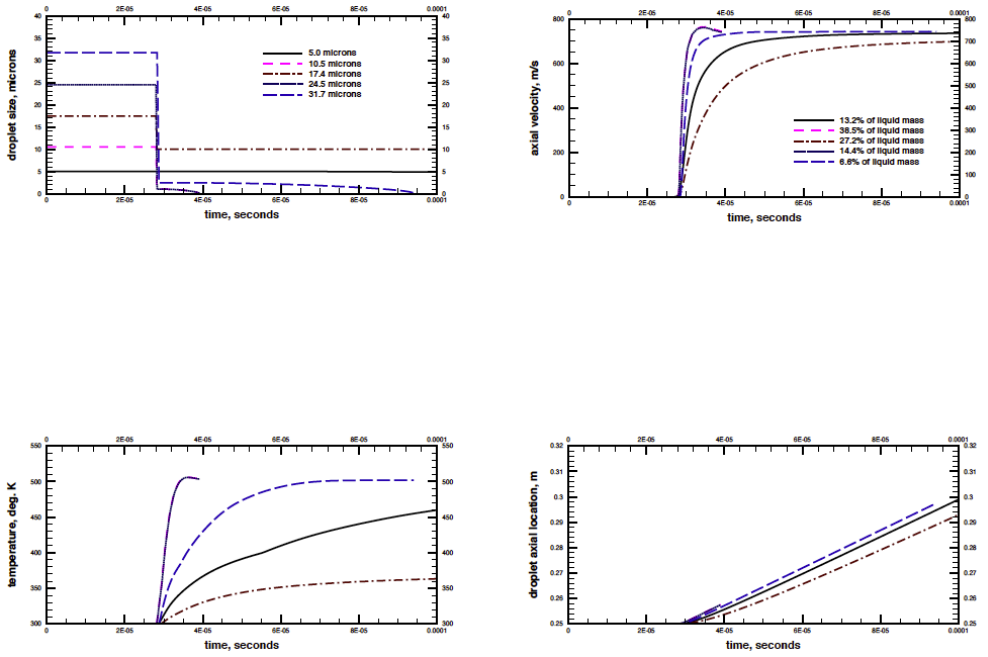

Fig. 11 Shock induced droplet behavior for an injector condition based on DSD of Banhawy et al. [20] with SMD = 15 microns.

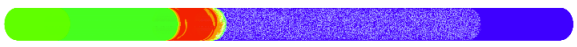

Fig. 12 Simualtion geometry.

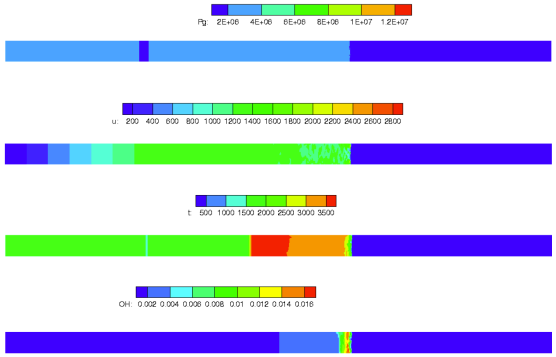

Fig. 13 Contour plots of pressure, axial velocity, temperature, & OH (gaseous, $\phi = 1.0$).

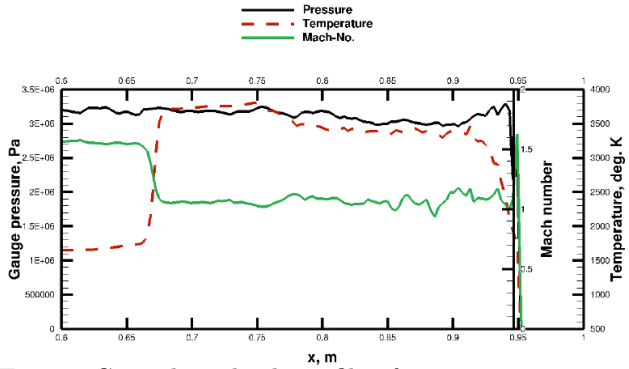

Fig. 14 Centerline shock profile of pressure, temperature, & Mach number (gaseous, $\phi = 1.0$).

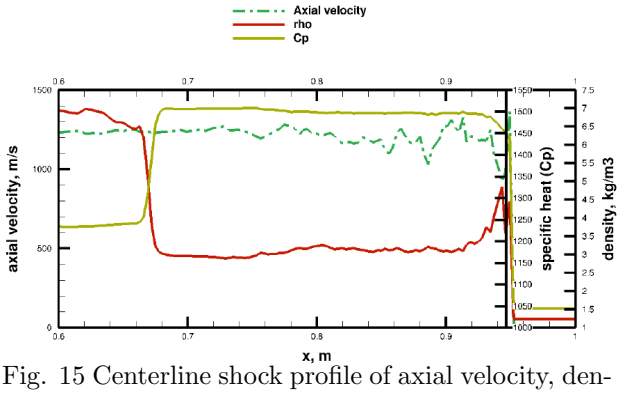

Fig. 15 Centerline shock profile of axial velocity, density, & specific heat (gaseous, $\phi = 1.0$).

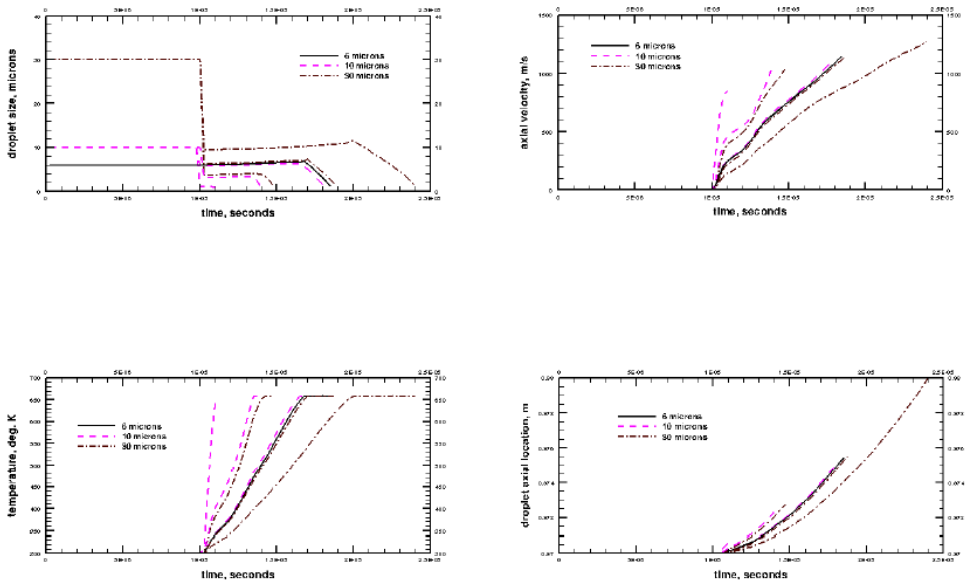

Fig. 16 Shock induced droplet behavior under reacting conditions of a sparse group of individual droplets (6, 10, & 30 microns).

Results on Individual Droplet Behavior

Next we are going to show some results undertaken to study individual droplet behavior by introducing a sparse group of 9 individual droplets. They are initially placed at an axial location of 0.97 m just before an approaching detonation front. They are comprised of three of each initial-size droplets of 6, 10, & 30 μm. It is important to note that following the passage of the detonation front, vaporization takes place under supercritical conditions since the critical pressure of $C_{11}H_{21}$ is 18.2 atm. The time variation of droplet size, axial velocity, liquid temperature, & axial location are shown in Fig. 16. While the smaller droplets (6-μm) remain unaffected by shock-induced secondary breakup, the 30-μm droplets are broken up into sizes ranging from 6 to 10 μm and the 10-μm droplets into 1 to 6 μm. As expected, smaller droplets accelerate much faster. Also, they evaporate faster before even approaching the corresponding gas velocity, 1300 m/s. Only the largest (10μm-child) droplets seem to reach that velocity. It is worth noting that the liquid temperature is capped currently at 650 K instead of allowing it to reach the critical temperate of $C_{11}H_{21}$, 658 K, in order to avoid some anticipated numerical issues. Under normal sub-critical engine operating conditions, it typically takes about 0.9 ms (90e-05 s) for a 30-μm droplet to evaporate completely and 0.36 ms (3.6e-05 s) for a 6-μm droplet. In our present calculations, it is less than 2.5e-05 s for a 30-μm droplet (aided by secondary breakup) & 1.8e-05 s for a 6-μm droplet. The time variation of droplet axial location shows that the smaller droplets stay closer to the shock front before they evaporate. Before complete vaporization, the largest droplets (10μm) traverse the most from their initial location by about 10 mm and others well below 6 mm. Considering that the detonation front also traverses by about 3 cm during the same period, most of the evaporation is completed well within 2 cm from the detonation front. It is well within the region of complete combustion. The results seem to indicate that the overall detonation properties of a droplet cloud made up of 6 to 30 microns are likely to be similar to those observed in a gaseous fuel/air mixture.

Results involving a Droplet Cloud

In this section, the results involving a mixed-phase fuel (70% liquid & 30% gas)/air mixture are presented. In our present calculations to save some computational time, the last section of the shock tube (0.5 to 1.5 m) is only filled partially with a droplet cloud (0.5 to 1.25 m). It is made up of 250,000 droplets with an initial liquid temperature of 300 K. First we are going to show some results from a cloud

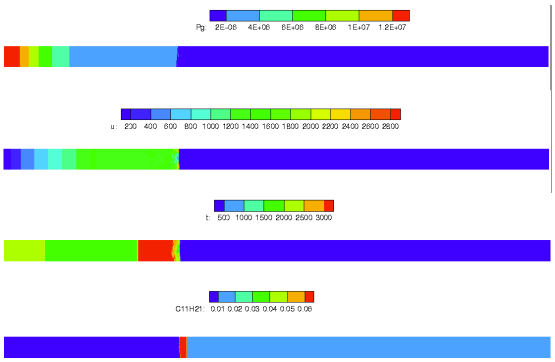

Fig. 17 Contour plots of pressure, axial velocity, temperature, & $C_{11}H_{21}$ (70% liquid [10 μm] & 30% gas, $\phi = 1.0$).

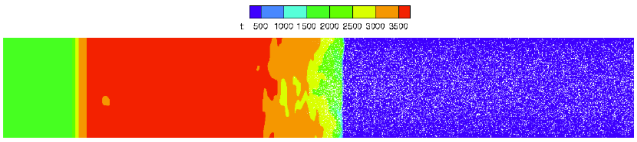

Fig. 18 Enlarged contour plot of temperature (70% liquid [10 μm] & 30% gas, $\phi = 1.0$).

made up of 10 μm droplets. The starting point for all the droplet-cloud calculations is the same. A droplet cloud is introduced into a calculation just before the shock front is about to enter the last section of the shock tube. The contour plots of pressure, axial velocity, temperature, & $C_{11}H_{21}$ (70% liquid & 30% gas, $\phi = 1.0$) at this location are shown in Fig. 17.

An enlarged sectional view of the temperature contour plot taken during a middle of shock propagation through the cloud is shown Fig. 18. As can be seen from the scatter plot of droplets, most the evaporation takes place within a short distance from the shock front. Again, the results seem to indicate that the detonation properties of this droplet cloud is likely to be similar to those observed in a gaseous calculation. Next, the contour plots of pressure, axial velocity, temperature, & OH near the end of this calculation are shown in Fig. 19. It also contains the scatter plot of droplets. The corresponding centerline shock profile of gas-phase gauge pressure,

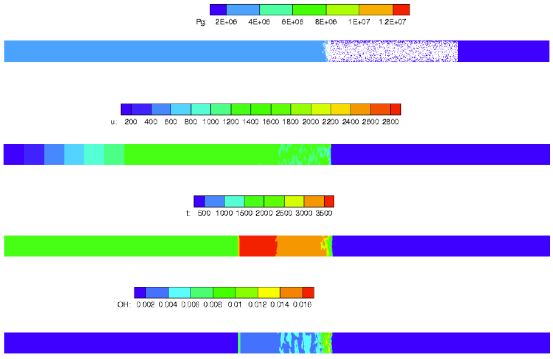

Fig. 19 Contour plots of pressure, axial velocity, temperature, & OH (70% liquid [10 μm] & 30% gas, $\phi = 1.0$).

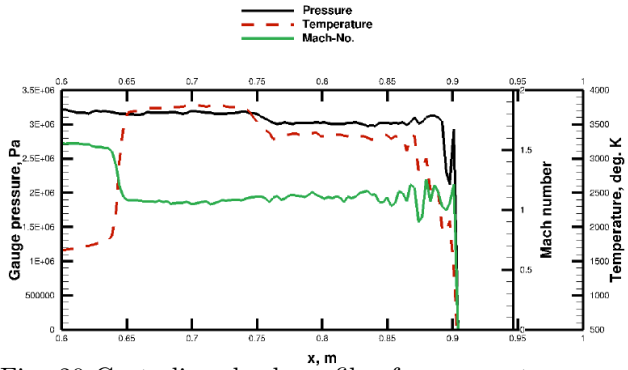

Fig. 20 Centerline shock profile of pressure, temperature, & Mach number (70% liquid [10 μm] & 30% gas, $\phi = 1.0$)).

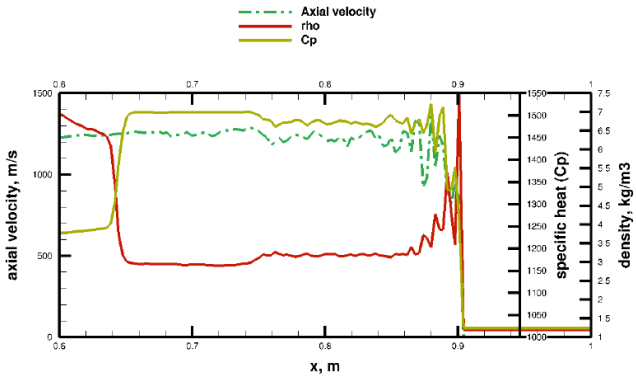

Fig. 21 Centerline shock profile of axial velocity, density, & specific heat (70% liquid [10 μm] & 30% gas, $\phi = 1.0$)).

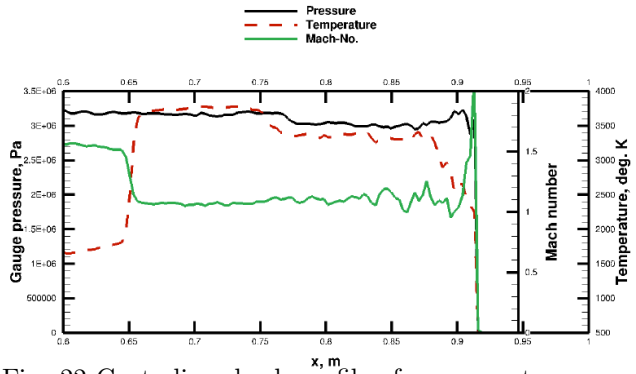

Fig. 22 Centerline shock profile of pressure, temperature, & Mach number (70% liquid [30 μm] & 30% gas, $\phi = 1.0$)).

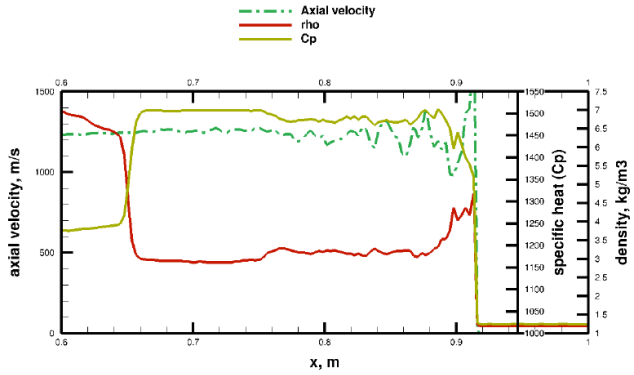

Fig. 23 Centerline shock profile of axial velocity, density, & specific heat (70% liquid [30 μm] & 30% gas, $\phi = 1.0$)).

temperature, Mach number, axial velocity, density and C_p are shown in Figs. 20 & 21. Away from the flame region, the results are mostly similar to those observed ear-lier in the gaseous calculation. The centerline shock profiles from the 30-μm droplet cloud are shown in Figs. 22 & 23 and those from the 6-μm cloud in Figs. 24 & 25. They also show similar behavior.

Finally, the calculated detonation velocities are summarized in Table 1. For this overdriven condition, the detonation velocity is 2044 m/s in the calculation involving a gaseous fuel. In those with mixed-phase, the calculated detonation speeds are 2013.8, 2000 & 1972 m/s for clouds made up of 6, 10, & 30 microns, respectively. The effect of increased droplet size is primarily seen in a slight reduction in the detona-tion velocity. However, its impact is not that signif-icant because of the rapid liquid vaporization result-ing from both shock-induced droplet breakup & prevailing supercritical conditions behind the detonation front.

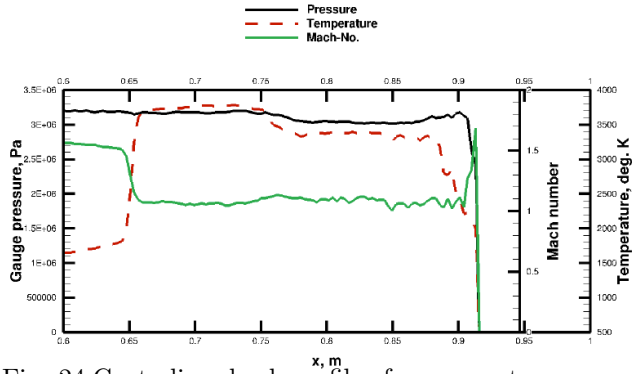

Fig. 24 Centerline shock profile of pressure, temperature, & Mach number (70% liquid [6 μm] & 30% gas, $\phi = 1.0$)).

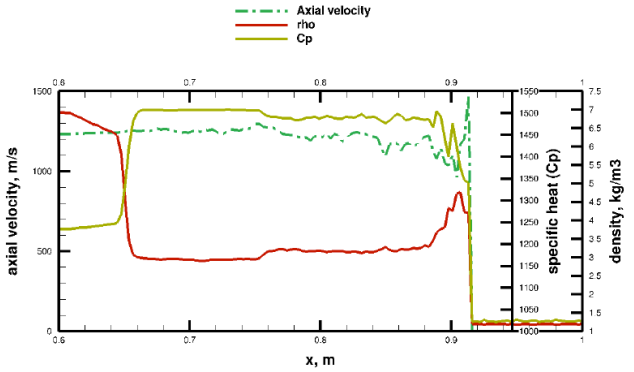

Fig. 25 Centerline shock profile of axial velocity, density, & specific heat (70% liquid [6 μm] & 30% gas, $\phi = 1.0$)).

Table 1. Detonation velocity (m/s) comparisons.				
Calculations	(1)	(2)	(3)	(4)
	all gaseous ($\phi = 1.0$)	70% liquid & 30% gas ($\phi = 1.0$)		
		6 μm	10 μm	30 μm
Predicted	2044	2014	2000	1972

C-J Detonation

In this section, we present the results obtained from a lower pressure test condition of 50 atm in the driver section of the shock tube.

Results Involving a Gaseous Fuel/Air Mixture

The contour plots of plots of gauge pressure, axial velocity, gas temperature, $C_{11}H_{21}$ are shown in Fig. 26. The corresponding centerline shock profile of gas-phase gauge pressure, temperature, Mach number, axial velocity, density and C_p are shown in Figs. 27 & 28. The shock profile is similar to what one expects from a ZND (Zeldovich, Neumann, & Doring) model but for one major exception. Absent from this calculation is the expected sharp pressure rise associated with the Von Neumann spike of 33 atm [29]. In our present calculations it plateaued at about 25 atm (in the preheat zone). The reasons for this discrepancy could be attributed to the coarser grid employed in our 3D calculations. Following the shock front, the flow expands until it reaches a stable state where the calculated values for P_g, T_g, & axial velocity are about 18 atm, 3000 K, & 700 m/s, respectively. Most of combustion is completed within a region of about 4 cm. The calculated detonation velocity is 1822 m/s which is close to the C-J detonation velocity reported by [29] for Jet-A/air at $\phi = 1$.

Results on Individual Droplet Behavior

Next we are going to show some results on the individual droplet behavior by introducing a sparse group of droplets similar to what we have done in a prior calculation. The time variation of their droplet behavior is shown in Fig. 29. Also, it is important to note that vaporization again takes place under supercritical conditions. The resulting shock induced break behavior is similar to what we observed earlier in Fig. 16. However, it takes a slightly longer time

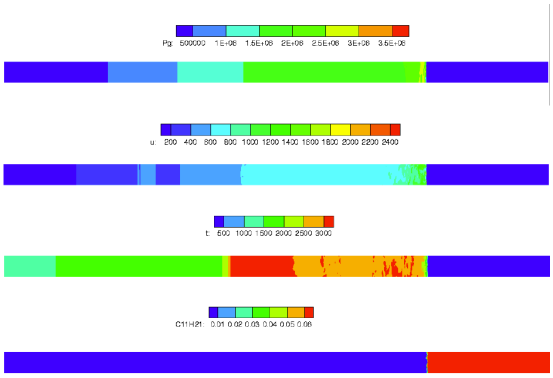

Fig. 26 Contour plots of pressure, axial velocity, temperature, & $C_{11}H_{21}$ (gaseous, $\phi = 1.0$).

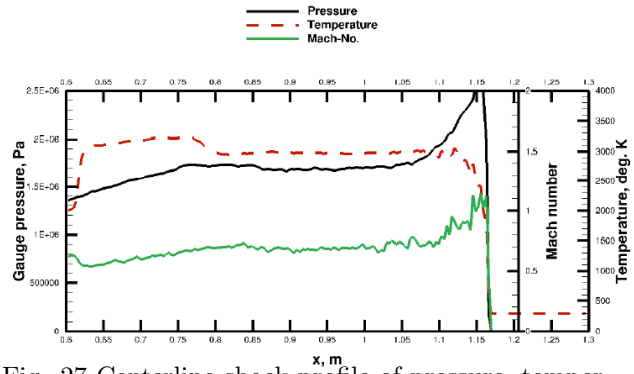

Fig. 27 Centerline shock profile of pressure, temperature, & Mach number (gaseous, $\phi = 1.0$).

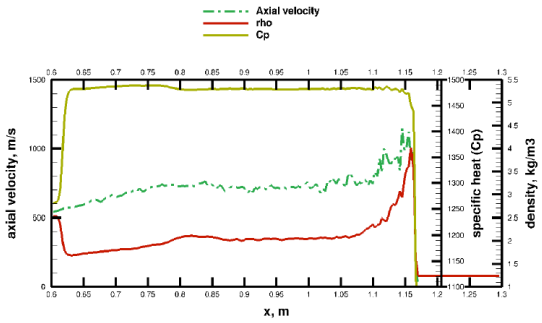

Fig. 28 Centerline shock profile of axial velocity, density, & specific heat (gaseous, $\phi = 1.0$).

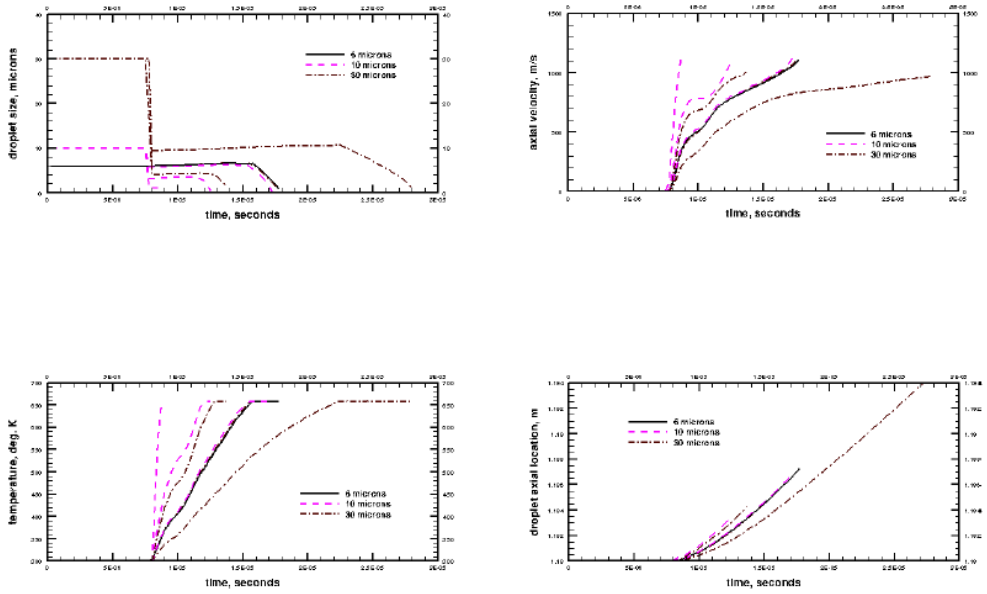

Fig. 29 Shock induced droplet behavior under reacting conditions of a sparse group of individual droplets (6, 10, & 30 microns).

for complete vaporization of all droplets (3e-5 s as compared to 2.5e-5 s). While the largest of droplets (10 μm) traverse longer (14 mm), all others vaporize within a short distance of 7 mm. Considering that the detonation front also traverses by about 3.65 cm during the same period, most of the evaporation is completed well within 2.15 cm from the detonation front. It is well within the region of complete combustion. Again, the results seem to indicate that the overall detonation properties of a droplet cloud made up of 6 to 30 microns are likely to be similar to those observed in a corresponding gaseous fuel/air mixture.

Results involving a Droplet Cloud

In this section, we present the results undertaken to study shock propagation through a a mixed-phase fuel (70% liquid & 30% gas)/air mixture. First we are going to show the results obtained from a cloud made up of 30-μm droplets. The contour plots of pressure, axial velocity, temperature, & $C_{11}H_{21}$ are shown in Fig. 30. It also contains the scatter plot of droplets. The corresponding centerline shock profile of gauge pressure, temperature, Mach number, axial velocity, density and C_p are shown in Figs. 31 & 32. Away from the flame region, the results are mostly similar to those observed earlier in a corresponding gaseous calculation. The centerline shock

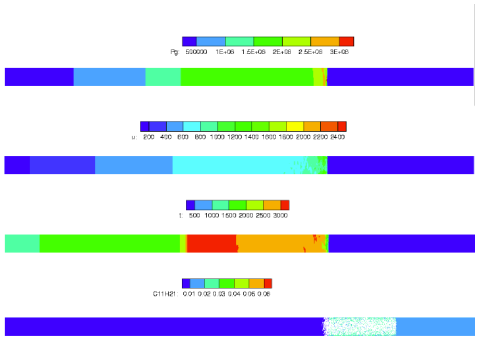

Fig. 30 Contour plots of pressure, axial velocity, temperature, & C11H21 (70% liquid [30 μm] & 30% gas, $\phi = 1.0$).

profiles from a 6-μm droplet cloud are shown in Figs. 33 & 34. They also show similar behavior.

Finally, the detonation velocities from the 50–atm (driver section) calculations are summarized in Table 2. In the calculation involving a gaseous fuel, the detonation velocity is 1822 m/s. In those with droplet clouds of 6 & 30 μm, the detonation speeds are 1800 & 1779 m/s, respectively. Again, the effect of increased droplet size is primarily seen in a slight reduction in the detonation velocity.

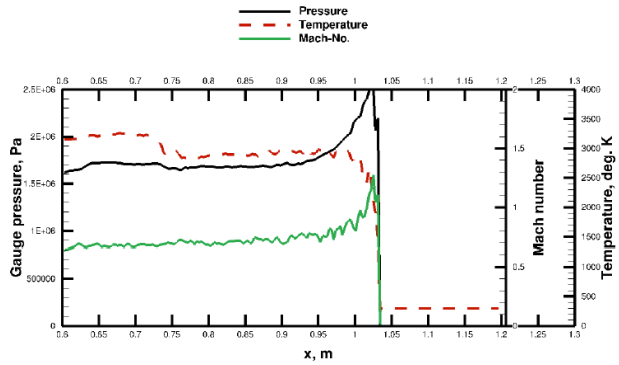

Fig. 31 Centerline shock profile of pressure, temperature, & Mach number (70% liquid [30 μm] & 30% gas, $\phi = 1.0$)).

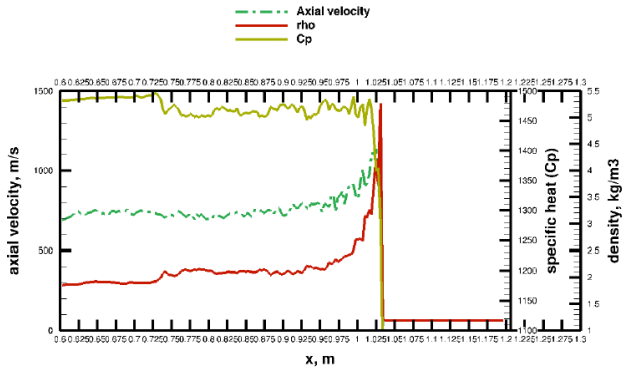

Fig. 32 Centerline shock profile of axial velocity, density, & specific heat (70% liquid [30 μm] & 30% gas, $\phi = 1.0$)).

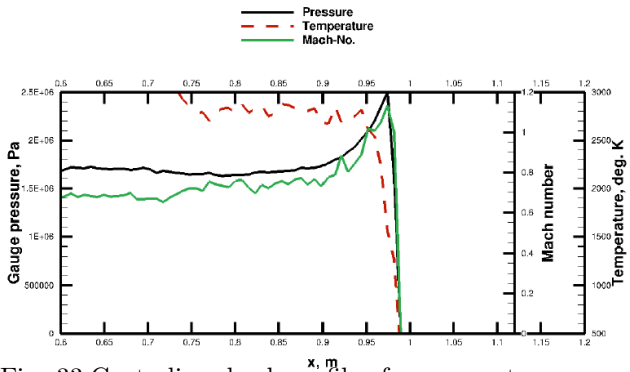

Fig. 33 Centerline shock profile of pressure, temperature, & Mach number (70% liquid [6 μm] & 30% gas, $\phi = 1.0$)).

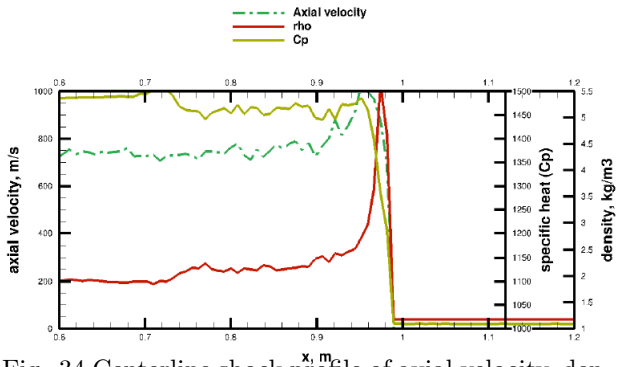

Fig. 34 Centerline shock profile of axial velocity, density, & specific heat (70% liquid [6 μm] & 30% gas, $\phi = 1.0$)).

Table 2 Detonation velocity (m/s) comparisons.			
Calculations	(1)	(2)	(3)
	all gaseous ($\phi = 1.0$)	70% liquid & 30% gas ($\phi = 1.0$)	
		6 μm	30 μm
Predicted	1822	1792	1779

6. CONCLUDING REMARKS

The paper describes the details of a spray modeling approach developed for use in the numerical simulations of multi-phase compressible flows. In an effort to extend our current capability of OpenNCC for application in the RDE technology enablement project at NASA GRC, we completed the implementation of a modeling approach for shock-induced droplet breakup & shattering based on the criteria developed by Borisov et al. [3]. In our current implementation, the actual droplet outcomes are determined by the existing RT (Rayleigh-Taylor) and ETAB (Enhanced Taylor Analogy Breakup) secondary droplet breakup models as described in LSPRAY-V [20]. Also, we completed the implementation of a vaporization model valid over a wide range of pressure conditions encountered in multiphase detonation.

Following its implementation, several numerical simulations were performed based on a simple rectangular shock-tube configuration in order to gain some understanding of individual droplet behavior followed by the passage of a shock front under non-reacting conditions. The calculations were carried out by tracking a sparse group of Jet-A ($C_{11}H_{21}$) droplets (five to ten) after placing them once before an incoming incident shock. In a wide range of subcritical conditions investigated over various fuel injector conditions & shock strengths, larger droplets

are noticed to undergo significant changes in droplet behavior following their breakup. However, smaller droplets (less than 10 μm) remain unaffected by any shock-induced breakup.

In a separate study, we investigated the impact of shock and droplet interaction in a detonation study involving both gaseous & mixed-phase (30% gas & 70% liquid) fuel/air stoichiometric mixtures in a simple 3D shock-tube configuration. In the mixed-phase calculations, the multi-phase fuel is comprised of a droplet cloud. Also, in order to gain some understanding of individual droplet behavior, the behavior & movement of a sparse group of droplets is examined in a calculation involving a gaseous fuel/air mixture. The results represent conditions that lead to both overdriven detonation and C-J detonation velocities. Under both test conditions, most of the droplet vaporization takes place well within in a short distance behind the detonation front. The overall detonation properties are mostly similar in both gaseous and droplet clouds. In the calculations involving droplet clouds, the detonation velocities are lower than in a corresponding gaseous fuel/air mixture. The impact of increased droplet size is primarily seen in a higher reduction in the detonation velocity.

Finally, we conclude the paper by identifying some important aspects that need to be addressed in a future study:

- There is a need for relevant experimental data for validation purposes.

- Currently, the reacting calculations (undertaken to investigate multi-phase detonation) are performed by making use of a coarse grid with an axial spacing of 0.05 cm & 0.0296 cm in the circular direction. Consequently, some important aspects of C-J detonation such as the pressure rise associated with the Von Neumann spike are not properly resolved.

REFERENCES

1. K. Kailasanath, "Liquid-Fueled Detonations in Tubes," Journal of Propulsion and Power, Vol. 22, No. 6, 2006.

2. E. K. Dabora, K. W. Ragland, and J. A. Nicholls, "A Study of Heterogeneous Detonations," Astronautica Acta, Vol. 12, No. 1, pp. 9-16, 1966.

3. A. A. Borisov, B. E. Gel'fand, M. S. Natanzon, and O. M. Kossov, "Droplet Breakup Regimes and Criteria," Journal of Engineering Physics, Vol. 40, pp. 4449 (1981).

4. K. W. Ragland, E. K. Dabora, and J. A. Nicholls, "Observed Structure of Spray Detonations," The Physics of Fluids 11, 2377 (1968).

5. R. Akbar, P. A. Thibault, P. O. Harris, L.-S. Lussier, F. Zhang, S.B. Murray & K. Gerrard, "Detonation Properties of Unsensitized and Sensitized JP-10 and Jet-A Fuels in Air for Pulse Detonation Engines." AIAA-2000-3592, 2000.

6. F. R. Schauer, C. L. Miser, K. C. Tucker, R. P. Bradley, & J. L. Hoke, "Detonation Initiation of Hydrocarbon-Air Mixtures in a Pulsed Detonation Engine," AIAA-2005-1343, 43rd AIAA Aerospace Sciences Meeting, January 10-13, 2005, Reno NV.

7. C. M. Brophy, J. O. Sinibaidi, D. W. Netzer, & R. G. Johnson, "Operation of a JP-10/Air Pulse Detonation Engine," AIAA 2000-3591, 36th AlAA/ASME/SAE/ASEE Joint Propulsion Conference, 17-19 July 2000, Huntsville, Alabama.

8. S. S. Vasu, D. F. Davidson, & R. K. Hanson. "Jet fuel ignition delay times: Shock tube experiments over wide conditions and surrogate model predictions," Combustion & Flame, vol.152, pp.125-143, 2008.

9. J. Kersey, E. Loth, & D. Lankford, "Effects of Evaporating Droplets on Shock Waves," AIAA Journal, Vol. 48, No. 9, September 2010.

10. E. J. Chang, & K. Kailasanath, "Shock wave interactions with particles and liquid fuel droplets." Shock Waves, vol. 12, pp. 333-341, (2003).

11. S. Cheatham & K. Kailasanath, "Numerical Simulations of Multiphase Detonations," 41st Aerospace Sciences Meeting and Exhibit, 6-9 January 2003, Reno, Nevada.

12. S. Sivier, E. Loth, J. Baum, & R. Lohner, "Unstructured adaptive re-meshing finite element method for dusty shock flow," Shock Waves, vol. 4, pp. 15-23, 1994.

13. G. Jourdan, L. Biamino, C. Mariani, C. Blanchot, E. Daniel, J. Massoni, L. Houas, R. Tosello, & D. Praguine, "Attenuation of a shock wave passing through a cloud of water droplets," Shock Waves, vol. 20, pp. 285-296, 2010.

14. K. Balakrishnan, & S. Menon, "Simulation Of Blast Wave Propagation and Particle Motion from Detonation Containing Dense Inert Particles," AIAA 2008-4689, 44th AIAA/ASME/SAE/ASEE Joint Propulsion Conference & Exhibit, 21-23 July 2008, Hartford, CT.

15. V. B. Nguyen, J.-.M. Li, T.-C. Juay, & B.-C. Khoo, "Numerical Simulation of Combustion Process for Two-Phase Fuel Flows Related to Pulse Detonation Engines," 30th International Symposium on Shock Waves, vol. 1, pp 397-403, 11 August, 2017.

16. A. K. Hayashi, N. Tsuboi, & E. Dzieminska, "Numerical Study on JP-10/Air Detonation and Rotating Detonation Engine," AIAA Journal, Vol. 58, No. 12, December 2020.

17. Y. Ling , A. Haselbacher , S. Balachandar , F. M. Najjar , & D. S. Stewart, "Shock interaction with a deformable particle: Direct numerical simulation and point-particle modeling," Journal of Applied Physics, Vol. 113, 2013.

18. A. A. Ranger, & J. A. Nicholls, " Aerodynamic Shattering of Liquid Drops," AIAA Journal, Vol.7, pp.285-291, 1969.

19. C. Segal, A. Chandy, & D. Mikolaitis, "Breakup of Droplets Under Shock Impact," Combustion Processes in Propulsion (control, Noise, and Detonation), Chapter 6, pp. 321-328, Butterworth & Heinemann, 2006.

20. M. S. Raju, "LSPRAY-V: A Lagrangian Spray Module," NASA/CR-2015-218918, NASA Glenn Research Center, Cleveland, Ohio, November, 2015.

21. F. X. Tanner, "Liquid Jet Atomization and Droplet Breakup Modeling of Non-evaporating Diesel Fuel sprays," SAE Technical Paper 970050, 1998. Also, appeared as SAE 1997 Transactions: Journal of Engines, Vol. 106, Sec. 3, pp. 127-140, 1998.

22. F. X. Tanner, "A Cascade Atomization and Drop Breakup Model for the Simulation of High-Pressure Liquid Jets," SAE Paper 2003-01-1044, 2003.

23. M. A. Patterson, and R.D. Reitz, "Modeling the Effects of Fuel Characteristics on Diesel Engine Combustion and Emissions," SAE 980131, 1998.

24. N.-S. Liu, T.-H. Shih, & C. T. Wey, "Comprehensive Combustion Modeling and Simulation: Recent Progress at NASA Glenn Research Center," ISABE-2007-1268, 18th International Symposium on Air Breathing Engines, Beijing, China, September 2-7, 2007.

25. M. S. Raju, "EUPDF-II - An Eulerian-Based Monte Carlo Probability Density Function (PDF) Solver - User's Manual," NASA/CR-2004-213073, NASA Lewis Research Center, Cleveland, Ohio.

26. M. S. Raju, J. P. Moder, & C. T. Wey, "Preliminary Soot Computations Based on a Model Aircraft Combustor With OpenNCC," ISABE-2019-24007, 24th International Symposium on Air Breathing Engines, Canberra, Australia, September 22-27, 2019.

27. K. Ajmani, K. Kundu, & P. F. Penko, "A study on detonation of JET-A using reduced mechanism," 48th AIAA Aerospace Science Meeting Including the New Horizons Forum and Aerospace Exposition, Orlando, FL, 4-7 January, (2010).

28. M. Sommerfeld, "The unsteadiness of shock waves propagating through gas-particle mixtures," Experiments in Fluids, 3, pp.197-206 (1985).

29. S. Yungster, & K. Breisacher, "Study of NOx Formation in Hydrocarbon-Fueled Pulse Detonation Engines," 41st AIAA/ASME/SAE/ASEE Joint Propulsion Conference, 10-13 July, 2005, Tucson, AZ.